www.sciencemag.org/cgi/content/full/324/5928/759/DC1

Supporting Online Material for

Representation of Confidence Associated with a Decision by Neurons in the Parietal Cortex

Roozbeh Kiani and Michael N. Shadlen

E-mail: roozbeh@u.washington.edu (R.K.); shadlen@u.washington.edu (M.N.S.)

Published 8 May 2009, *Science* **324**, 759 (2009)
DOI: 10.1126/science.1169405

This PDF file includes:

Supplementary Online Material

Materials and Methods

Behavioral task

We measured the choice certainty in a direction discrimination task using a post-decision wagering design (Fig. 1A). Two adult rhesus monkeys (*Macaca mulatta*) were trained to judge the net direction of a field of dynamic random dots (*S1, S2*). Task difficulty was controlled by varying the viewing duration (100-900 ms, truncated exponential distribution) and the percentage of coherently moving dots (motion strength) as described previously (*20, S3*). After extinction of the motion display, the monkeys held fixation through a delay period (1200-1800 ms) before extinction of the fixation point. On a random half of the trials, a third target (sure target, T_s) appeared at a random time during the delay period (500-750 ms after motion offset) and stayed on through the delay period. After extinction of the fixation point, the monkey indicated its choice by making a saccadic eye movement either to one of the two direction targets or to T_s, if present. The monkey received a liquid reward for a correct choice, and nothing plus a short timeout for an error. Choosing T_s, when present, always yielded a reward, but the reward size was smaller than that for a correct response. The reward ratio was adjusted to encourage the monkey to choose the sure target on nearly half of all trials in order to increase the statistical power of analyses on neural responses. The sure bet allowed the monkey to opt out of the high stakes decisions about motion direction.

We collected 150,558 trials (45,989 psychophysics and electrophysiology trials, and 104,569 psychophysics trials) from two monkeys in 200 experimental sessions. Across the sessions, the ratio of reward size for the sure bet and the high-stakes decisions was 0.79±0.07 (median=0.81). On 114 sessions half of the trials for each motion strength shared a fixed seed for the random number generator. The fixed seed guaranteed a fixed sequence of motion by eliminating trial-to-trial variation of the stimulus frames. We collected 83,809 trials in these sessions (35,023 psychophysics and electrophysiology trials, and 48,786 psychophysics trials).

In electrophysiology sessions, we recorded the activity of single neurons in the ventral division of area LIP (LIPv) (*S4*) while the monkey performed the task. Standard electrophysiology techniques were used for these extracellular recordings (*20, 21*). LIPv was identified by three characteristic markers: (1) anatomical location, confirmed by stereotactical location and by registering the monkey's structural MRI scans with a high resolution "flattened" scan distributed with the CARET software package (*S5*); (2) transition of white and gray matter during recordings; and (3) sustained activity of neurons in delayed and memory guided saccade tasks (*S6*). We screened 81 neurons with sustained activity in the vicinity of LIPv. All but 10 neurons were included in the analysis. The excluded neurons did not exhibit clear selectivity during the decision making. All training and data collection procedures conformed to the National Institutes

of Health *Guide for the Care and Use of Laboratory Animals* and were approved by the University of Washington Animal Care Committee.

Analysis of behavioral data

We used logistic regression to examine the effects of motion strength (c ; range 0 to 0.512) and duration (t ; 0.1 to 0.9 s) on the probability of choosing T_s:

$$P_{sure} = \left[1 + e^{-(\beta_0 + \beta_1 c + \beta_2 t)}\right]^{-1} \quad (1)$$

where β_i are fitted coefficients determined using maximum likelihood (binomial error). The same equation describes the effect of the stimuli on the probability of a correct choice:

$$P_{cor} = \left[1 + e^{-(\beta_0 + \beta_1 c + \beta_2 t)}\right]^{-1} \quad (2)$$

To assess the improvement in accuracy when T_s was presented but waived, we extended Equation 2 as follows:

$$P_{cor} = \left[1 + e^{-(\beta_0 + \beta_1 c + \beta_2 t + \beta_3 I + \beta_4 cI + \beta_5 tI)}\right]^{-1} \qquad I = \begin{cases} 1, & T_s \text{ shown} \\ 0, & T_s \text{ not shown} \end{cases} \quad (3)$$

where I is an indicator variable. The null hypothesis is that probability correct does not change in the presence of T_s ($H_0 : \beta_{3-5} = 0$). This analysis supports our claim that by waiving T_s, accuracy improved at all motion strengths and durations (β_3 =0.12±0.03, p=0.00026; β_4 =1.28±0.14, $p<10^{-8}$; β_5 =0.88±0.33, p=0.008). For the last term, the analysis was limited to viewing durations under 300 ms, which is the range in which *t* has the largest effect on the probability correct (Fig. 1C) (β_5 was not significantly different from zero when longer durations were included).

To make Figures 1B-C and S1, trials were divided into 10% quantiles (deciles) based on stimulus duration for each motion strength. The probability of choosing T_s was calculated for each decile. Also, we calculated the probability of choosing the correct direction target when the monkey did not choose the sure target. We pooled 1.6% and 3.2% motion coherence to avoid clutter at the lower half of the figures, and because 1.6% coherence was tested only on some sessions. Note that all the statistical analyses were performed on individual trials, not on the deciles.

Bounded accumulation model

In this model, the discrimination of rightward and leftward motion directions is based on integration of noisy sensory evidence by two accumulators, which correspond to the two direction choices. The accumulated evidence is termed decision variable. The process continues until one of the accumulators reaches a fixed bound, or until the stream of motion evidence terminates, whichever happens first. The duration of the accumulation process is termed decision time. On trials in which T_s is not presented, the choice is

dictated by the accumulator that hits the bound first, or has the larger decision variable. The mechanism thus resembles a race between two accumulators. We can simplify the process further by assuming that a piece of evidence in favor of one of the options is against the other option. By this assumption, the fluctuations of decision variable in the two accumulators become anti-correlated and the race model reduces to a one-dimensional diffusion process in which the decision variable fluctuates in the space between the two decision bounds (*13, 39, S7*).

The propagation of the probability density of decision variable over time can be calculated using the Fokker-Planck equation (*S8*):

$$\frac{\partial p(v,t)}{\partial t} = \left[-\frac{\partial}{\partial v}\mu(v,t) + \frac{\partial^2}{\partial v^2} D(v,t) \right] p(v,t) \tag{4}$$

where $D(v,t)$ is the diffusion coefficient ($D(v,t) > 0$) and $\mu(v,t)$ the drift or advective coefficient. In the context of bounded accumulation models, $p(v,t)$ represents the probability of decision variable (v) at time t, $\mu(v,t)$ the strength of momentary evidence and $D(v,t)$ the variance of the momentary evidence. Based on previous studies (*S9, S10*) we assume that both the advective coefficient and the diffusion coefficient are stationary:

$$\begin{aligned} \mu(v,t) &= kc \\ D(v,t) &= 1 \end{aligned} \tag{5}$$

where k is a constant. The boundary conditions of the Fokker-Planck equation are:

$$p(v,t_0) = \delta(v) \tag{6}$$

and

$$p(\pm B,t) = 0 \tag{7}$$

which enforce the constraints that the initial value of the decision variable is zero and that the accumulation terminates whenever the decision variable reaches one of the bounds ($\pm B$).

In this model, there is an implicit mapping between the probability of a correct response and the value of decision variable. If $v(t)$ denotes the decision variable at decision time, the log posterior odds is

$$Log\frac{p(S_1 \mid v(t))}{p(S_2 \mid v(t))} = Log\frac{\sum_i p(v(t) \mid S_1, C_i)\, p(C_i \mid S_1)}{\sum_i p(v(t) \mid S_2, C_i)\, p(C_i \mid S_2)} + Log\frac{p(S_1)}{p(S_2)} \tag{8}$$

where S_1 and S_2 are the two motion directions, and C_i are the set of coherences used in the experiment. The two motion directions happen with equal frequency, and motion coherence and direction vary independently. Equation 8, therefore, is reduced to:

$$Log\frac{p(S_1 \mid v(t))}{p(S_2 \mid v(t))} = Log\frac{\sum_i p(v(t) \mid S_1, C_i)\, p(C_i)}{\sum_i p(v(t) \mid S_2, C_i)\, p(C_i)} \tag{9}$$

where $p(C_i)$ for $C_i = 0$ is half of other coherence levels. On trials in which T_s is presented, the model recommends choosing T_s when the absolute value of log posterior odds is less than a criterion level (θ).

Overall, there are three free parameters in the model: k, B, and θ. k and B are both expressed in units of the diffusion coefficient, and thus have arbitrary units. We fit these free parameters by maximizing the likelihood of the observed frequency of correct responses on trials in which T_s was not shown, and the observed frequency of choosing T_s on trials in which T_s was shown. The parameters were then used to predict the frequency of correct responses on trials in which the monkey waived T_s (solid lines in Fig. 4E). The fits were performed on individual trials using binomial error terms. The R^2 values for the goodness of fits or predictions were computed for the data points (deciles) shown on the Figures 4D-E.

To create the predicted trajectories of the decision variable (Fig. 4F), we performed a Monte-Carlo simulation of the diffusion process. The distribution of stimulus duration for the simulated trials was similar to that used in the experiment. To average the trajectory of the decision variable across the simulated trials, we assumed that the value of the decision variable at decision time is retained after the termination of the process and during the delay period that separates the motion stimulus from T_s onset.

Analysis of neural data

Peri-stimulus time histograms (PSTHs) shown in Figures 2, 4, 5, S2 and S4 were smoothed by convolution of neural responses with a 100 ms box car filter. However, all statistical analyses were performed on spike counts without any smoothing. To create population PSTHs in Figures 2, 4, S2, and S4 we normalized the activity of each neuron to the average firing rate of all trials in the 300 ms period before dots onset, that is the period after onset of the direction choice targets. For Figure 4F, the PSTHs were detrended by subtracting from each PSTH the mean of the correct T_{in} and T_{opp} PSTHs. For the population PSTH in Figure 5 (T_s in RF), responses were normalized to the average firing rate in the 300 ms period after T_s onset.

Single trial analyses were based on two measurements. The first was the neural activity calculated in a 200 ms window ending at T_s onset. The second was the rate of buildup in neural activity following motion onset. To calculate the buildup rate we first identified a relevant window for each cell, and then fit a line to neural responses in that window on each trial. The window started at the nadir (dip) of activity following motion onset and ended when the average firing rate achieved a steady level. The time of dip for each neuron was calculated as the time of minimum activity in 100-500 ms after motion onset (mean=195.8±9.4 ms). The beginning of steady level of activity was calculated for each cell by fitting the following ramp-to-plateau function after the dip to the average response for correct T_{in} choices.

$$r = \gamma_0 + \gamma_1 \min\{t, t_p\}$$

where r is the spike rate, t is time relative to the dip, and t_p is the beginning of the sustained level of activity; γ_i and t_p are free parameters. t_p, which defines the width of the window, was 299.9±7.6 ms across the population. Where necessary we trimmed the window to avoid overlap with the window used for the calculation of firing rate before T_s onset.

To test whether the buildup rate of activity is modulated by coherence we used the following regression

$$\dot{r} = \beta_0 + \beta_1 c \quad (10)$$

where $\dot{r}$ is buildup rate of activity for individual trials with correct T_{in} choices, and c is motion coherence. The null hypothesis is that buildup rate is not modulated by motion coherence ($H_0 : \beta_1 = 0$). When applied to the population of cells, buildup rates of the trials belonging to individual cells were first standardized by calculating z-scores (subtracting the mean and dividing by standard deviation).

We quantified the change of activity associated with the post-decision wager by comparing firing rates in the 200 ms epoch before onset of T_s on trials in which the monkey chose or waived this option. We show means and standard errors in Figures 2E-F and apply 2-sided t-tests to illustrate significant cases ($p<0.05$). Population summary statistics were based on two-way ANOVA with choice and cell identity as fixed and random effects, respectively.

We examined the variance of activity in the same 200 ms epoch before onset of T_s. If the mean firing rates associated with T_s choices arose from a mixture of values like those associated with the T_{in} and T_{opp} choices, then the ratio of the variance for all T_s choices is predicted to be equal to the variance of the pooled T_{in} and T_{opp} responses. Alternatively, if the mean represents the central tendency of an intermediate distribution, the variance should be smaller than this prediction. We performed an F-test to compare the variance of activity for T_s choices and the mixture of T_{in} and T_{opp} choices. For this analysis, neural responses on individual trials were standardized for each neuron and pooled across cells. Similar results were obtained by comparing the geometric mean of the variance ratios from each neuron to unity ($p=0.0004$, t-test on log transformed ratios). As a further test, we also used Monte Carlo methods to recreate the average delay activity for T_s choices by sampling, with appropriate proportions, from the distribution of activity for T_{in} and T_{opp} choices (*24*). The simulated distributions had larger variance than the observed distribution both for trials with T_{in} motion direction ($p<0.005$) and for trials with T_{opp} motion direction ($p<10^{-4}$).

To test how the deviation of neural activity from intermediate values on individual trials influenced the probability of choosing the sure target we used the following logistic regression:

$$P_{sure} = \left[1 + e^{-(\beta_0 + \beta_1 |z|)}\right]^{-1} \quad (11)$$

where $|z|$ is the magnitude (absolute value) of the standardized firing rate measured in the 200 ms epoch preceding onset of T_s. The standardization was applied to each neuron

using the mean and standard deviation across all trials, regardless of outcome. The logistic regression was applied to the population of z-transformed single-trial responses. The fitted coefficient β_1 quantifies the degree that deviation from intermediate firing rates affects log odds of choosing T_s. Our hypothesis is that larger deviations are associated with a lower probability of T_s choices ($H_0 : \beta_1 \geq 0$). We used a similar logistic regression for the effect of buildup rate, using standardized values of buildup rate from the same trials.

To test whether the single-trial effects were explained by motion strength and duration, we expanded Equation 11 to incorporate these terms and their interaction:

$$P_{sure} = \left[1 + e^{-(\beta_0 + \beta_1|z| + \beta_2 c + \beta_3 t + \beta_4 ct)}\right]^{-1} \quad (12)$$

The null hypothesis remains ($H_0 : \beta_1 = 0$).

To test if buildup rate during the decision making process conveyed information about the choice of sure target beyond what was conferred by the neural activity prior to sure target onset we used the following logistic regression.

$$P_{sure} = \left[1 + e^{-(\beta_0 + \beta_1|z_1| + \beta_2|z_2|)}\right]^{-1} \quad (13)$$

where z_1 and z_2 are standardized firing and buildup rates, as above. The null hypothesis is ($H_0 : \beta_2 = 0$).

Supplementary Figures

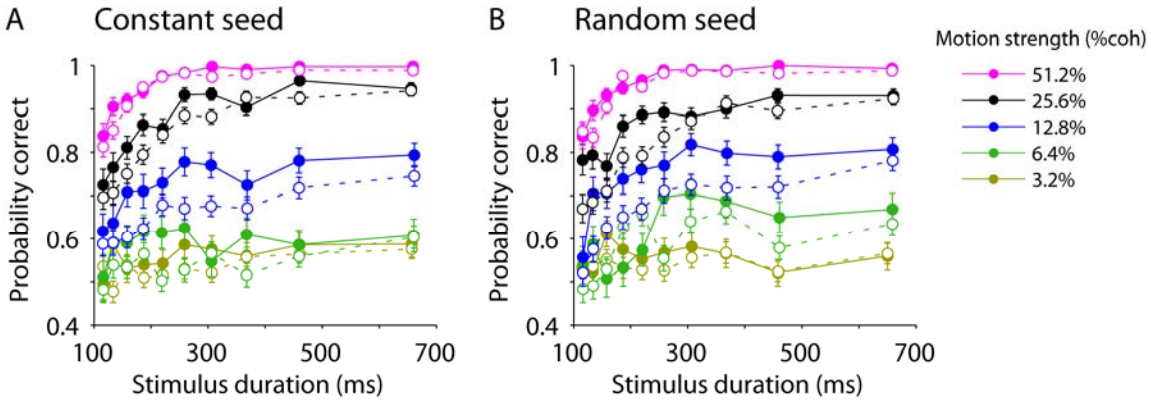

Figure S1.
Post-decision wagering reflects variability of neural signals as well as variation in stimulus difficulty. Here we show that the monkeys performed the task similarly on a subset of trials that used motion stimuli comprised of identical sequences of random dots. In some experimental sessions we used two trial types, which were randomly interleaved. For both trial types the probability of a correct response was larger when the monkey waived the sure target and chose the high stakes targets than when the monkey was not provided with the sure target. (A) Constant seed trials. An identical sequence of motion frames were shown for each motion strength. The trial-to-trial variability of stimulus was thus eliminated for these trials. (B) Random seed trials. The sequence of motion frames varied randomly from trial to trial.

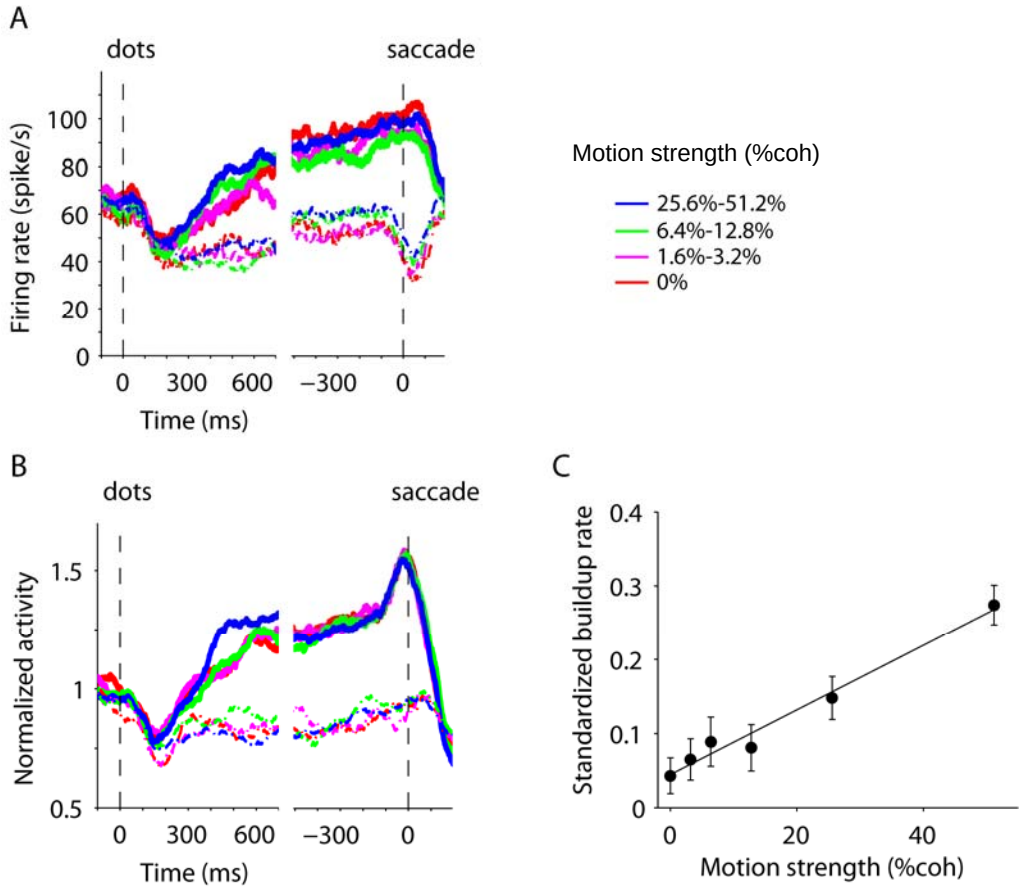

Figure S2.
The buildup of neural responses after motion onset was modulated by motion strength. (A) Responses of the example LIP neuron from Figure 2A-B. All conventions are similar to Figure 2A, except that trials are grouped by motion strength. After motion onset, the buildup of activity for T_{in} choices was larger for stronger motion stimuli. (B) Responses of the population of 70 LIP neurons. Same conventions as in A. The coherence-dependent increase in buildup rate is less evident because of the abundance of trials with short motion durations combined with variation in latency and magnitude of the buildup across neurons. These limitations are addressed in the next panel. (C) Standardized buildup rate across the population of neurons as a function of motion strength. Correct T_{in} choices, and all T_{in} choices for 0% motion strength, are included in this analysis. Buildup rates were calculated for single trials, as described in Methods, and then expressed as deviation from the mean in units of standard deviation. This procedure (standardization) was performed for each cell before pooling the data. The increase in buildup rate is well-described by a line fitted to the data. Error bars show SEM.

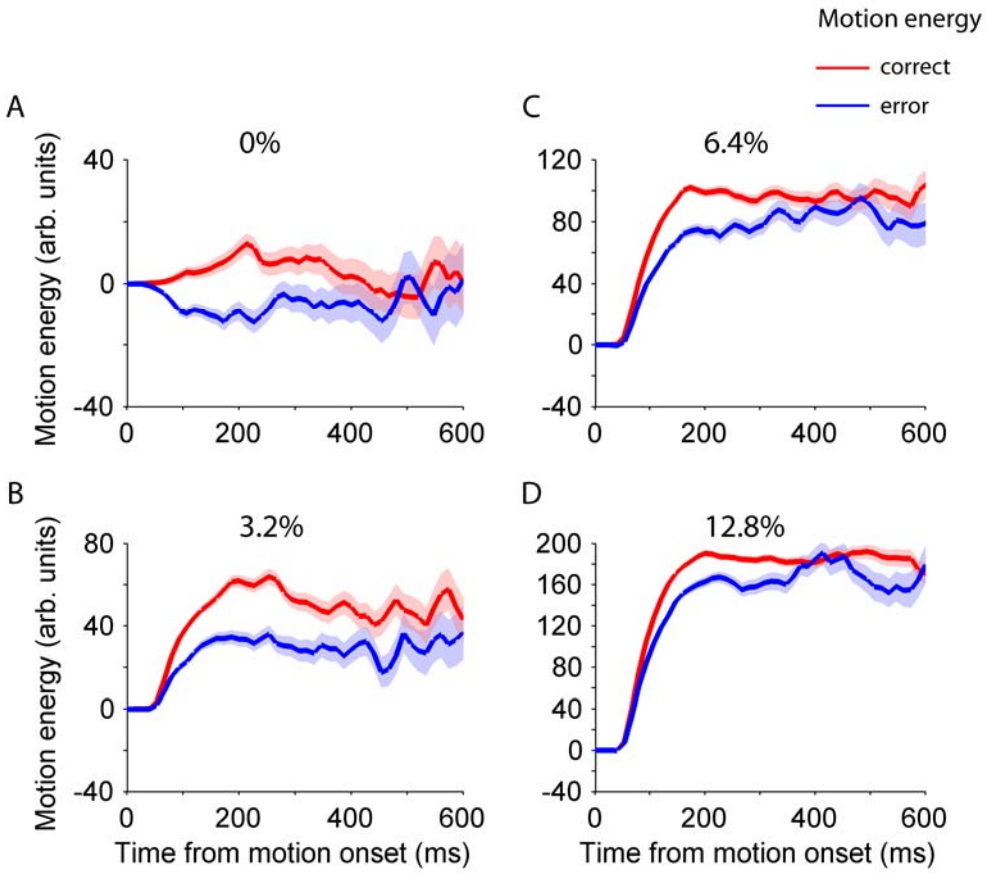

Figure S3.
Decision time is limited by a bounded evidence accumulation mechanism. The bounded accumulation model asserts a mechanism for terminating decisions. In reaction time tasks, this explains the relationship between decision speed and accuracy. In an experiment like ours, in which the stream of evidence is controlled by the experimenter, the mechanism asserts that some decisions terminate covertly, despite the availability of additional information from the stimulus. After the accumulated evidence reaches the bound, the incoming evidence would be largely ignored. Therefore, the initial part of the stimulus must have a larger influence on the monkey's choice. We performed a psychophysical reverse correlation analysis to test this assertion (*S11, S12*). On each trial, a particular random dot stimulus gave rise to a noisy stream of motion information, comprised of fluctuations in the magnitude and sign of evidence. These fluctuations were quantified by calculating the motion energy (*20, S13*). Positive motion energy indicates rightward motion for 0% coherence and motion in the 'correct' direction for non-zero coherences. The motion energy profiles for rightward and leftward choices (0% coherence, A) and correct and error choices (non-zero coherences, B-D) show a clear separation in support of the choice. The separation was clearest in the first ~400 ms, and overlapped at later times, consistent with a covert decision termination mechanism. Only trials with stimulus durations of 400 ms or larger contributed to this analysis.

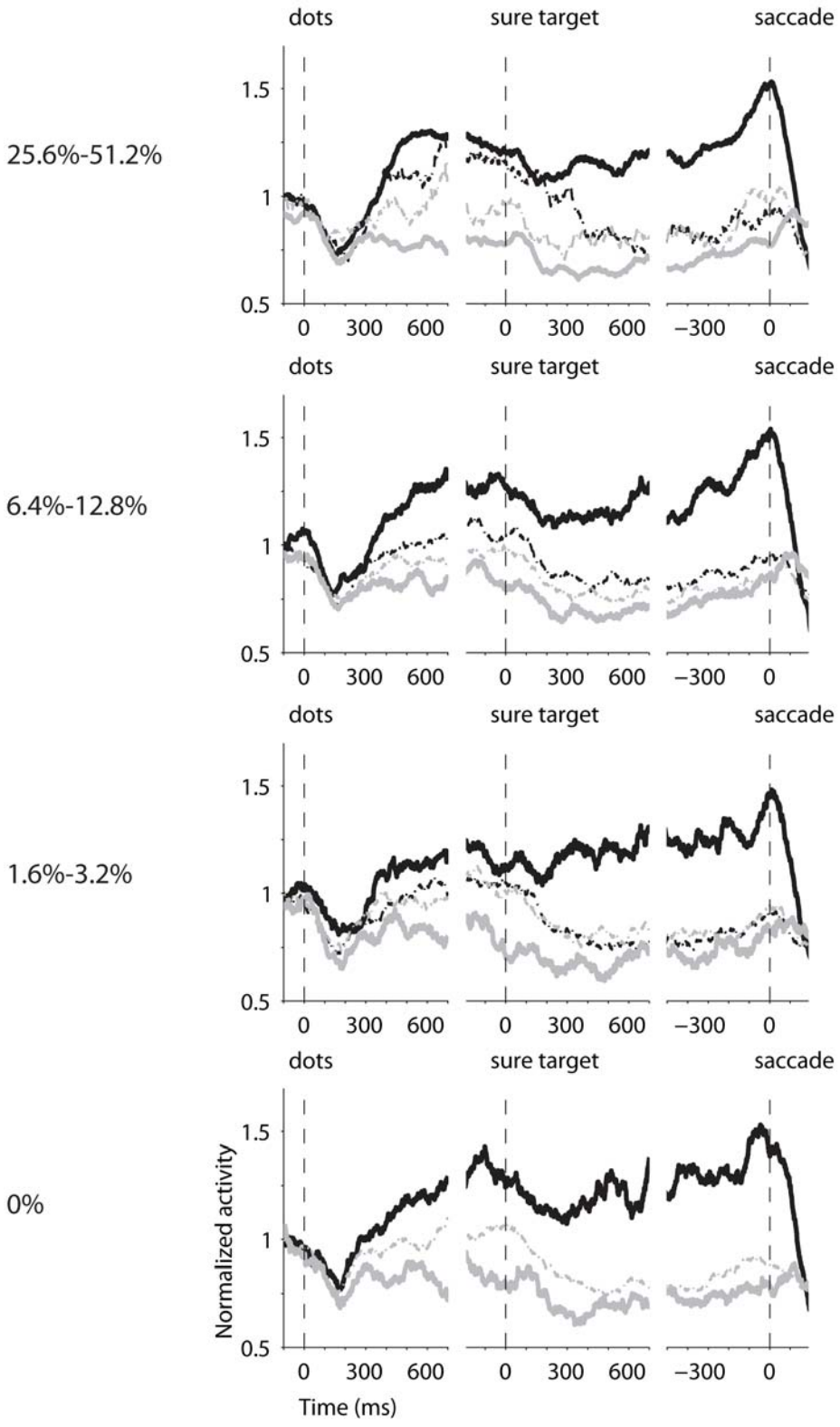

Figure S4.
The level of activity for T_s choices was modulated by motion strength. Population average responses from 70 LIP neurons are grouped by motion strength. One of the high stakes (direction choice) targets was in the RF of the recorded neurons. Plotting conventions are identical to Figure 2D. Coherence levels are paired for illustration purposes. The same trend exists for individual coherence levels.

Table S1. Fit parameters (mean±SE) of the bounded accumulation model.

k	0.255±0.002
B	39.4±10.0
θ	0.591±0.005

References

S1. W. T. Newsome, E. B. Pare, *J. Neurosci.* **8**, 2201 (1988).
S2. K. H. Britten, M. N. Shadlen, W. T. Newsome, J. A. Movshon, *J. Neurosci.* **12**, 4745 (1992).
S3. J. I. Gold, M. N. Shadlen, *J. Neurosci.* **23**, 632 (2003).
S4. J. W. Lewis, D. C. Van Essen, *J. Comp. Neurol.* **428**, 112 (2000).
S5. D. C. Van Essen, *Curr. Opin. Neurobiol.* **12**, 574 (2002).
S6. R. M. Bracewell, P. Mazzoni, S. Barash, R. A. Andersen, *J. Neurophysiol.* **76**, 1457 (1996).
S7. P. L. Smith, R. Ratcliff, *Trends Neurosci.* **27**, 161 (2004).
S8. S. Karlin, H. M. Taylor, *A second course in stochastic processes* (Academic Press, 1981).
S9. K. H. Britten, M. N. Shadlen, W. T. Newsome, J. A. Movshon, *Vis. Neurosci.* **10**, 1157 (1993).
S10. J. Ditterich, M. E. Mazurek, M. N. Shadlen, *Nat. Neurosci.* **6**, 891 (2003).
S11. P. Neri, *J. Vis.* **4**, 82 (2004).
S12. A. J. Ahumada, Jr., *J. Vis.* **2**, 121 (2002).
S13. E. H. Adelson, J. R. Bergen, *J. Opt. Soc. Am. A.* **2**, 284 (1985).